IEEE Access
Multidisciplinary | Rapid Review | Open Access Journal

Received April 12, 2019, accepted May 10, 2019, date of publication May 22, 2019, date of current version June 7, 2019.

Digital Object Identifier 10.1109/ACCESS.2019.2918286

Residual Water Suppression Using the Squared Eigenfunctions of the SchrÖdinger Operator

***ABDERRAZAK CHAHID[1], (Member, IEEE), *SOURAV BHADURI[2], MOHAMED MAOUI[1], ERIC ACHTEN[2], HACENE SERRAI[2,3], AND TAOUS-MERIEM LALEG-KIRATI[1], (Member, IEEE)**

[1]Computer Electrical and Mathematical Science and Engineering (CEMSE) Division, King Abdullah University of Science and Technology (KAUST), Thuwal 23955-6900, Saudi Arabia
[2]Department of Diagnostic Sciences, Ghent University, 9000 Ghent, Belgium
[3]Robarts Research Institute, The University of Western Ontario, London ON N6A 3K7, Canada

Corresponding author: Taous-Meriem Laleg-Kirati (taousmeriem.laleg@kaust.edu.sa)

This work was supported in part by the King Abdullah University of Science and Technology (KAUST) Base Research Fund under Grant BAS/1/1627-01-01, and in part by the Ghent University Funding.
**Abderrazak Chahid and Sourav Bhaduri are co-first authors.*

ABSTRACT Water suppression, in proton magnetic resonance spectroscopy (MRS) using post-processing techniques, is very challenging due to the large amplitude of the water line, which shadows the metabolic peaks with small amplitudes and complicates their quantification. In addition, the peak-shaped structure of these spectra and the relatively small number of data points representing them makes the suppression process more cumbersome. In this paper, a post-processing water suppression technique based on the Schrödinger operator is proposed. The method is based on the decomposition of the input MRS spectrum, using the squared eigenfunctions of a semi-classical Schrödinger operator. The proposed approach proceeds in three steps: first, the water peak is estimated using an optimal choice of the value of h to reconstruct the MRS spectrum with a minimum number of eigenfunctions. Second, these estimated eigenfunctions are further refined to ensure that they only represent the water line with no contribution from the metabolite peaks. Finally, the estimated water peak is subtracted from the input MRS spectrum. The proposed method is tested on simulated *in vitro* and real *in vivo* MRS data and compared with the Hankel–Lanczos singular value decomposition with partial reorthogonalization (HLSVD-PRO) method. The results obtained show that the semi-classical signal analysis (SCSA) performs comparably to the HLSVD-PRO in accurately suppressing the water peak.

INDEX TERMS Eigenfunctions of the Schrödinger operator, magnetic resonance spectroscopy, water suppression, digital signal processing.

I. INTRODUCTION

Biomedical signals consist of peaks, which reflect biological activities and chemical properties of the human body. Examples of such signals are Magnetic Resonance Spectroscopy (MRS) spectra, which allow the detection and quantification of highly concentrated brain metabolites, such as N-Acetyl-Aspartate (NAA), phospho-creatine (Cr) and Choline (Cho) [1]. In the case of abnormalities or in specific clinical conditions, some other metabolites can arise such as lactate (Lac) [2]. However, the quantification of these metabolites is usually hampered by the presence of a large water peak, which is of the order of 10000 compared to the metabolite resonances. Therefore, and for an appropriate metabolic quantification using ^{1}H-MRS, the suppression of the water line is required. The suppression can be achieved either during or after data acquisition, using either pre-processing or post-processing techniques, respectively. In the pre-processing scheme, water suppression is performed by a combination of frequency-selective saturation Radio-Frequency (RF) pulses and subsequent magnetic field gradients, played to saturate the water spins before acquisition of the metabolic signals. Among these techniques are CHESS [3], multiple pulses with optimized flip angles (WET) [4], variable power RF pulses with optimized relaxation (VAPOR) delays [5], and hyperbolic secant (HS) waveform as a 90 degrees saturation pulse [6]. Usually, the pre-processing water suppression techniques,

The associate editor coordinating the review of this manuscript and approving it for publication was Mohammad Zia Ur Rahman.

such as CHESS, significantly reduce the water peaks but they leave a residual water which affect the quantification. Moreover, the relevance of non-water-suppressed acquisition for intra-scan motion correction has been proven to avoid artifacts, which are induced due to the motion of the patient inside the scanner [7]. In addition, studies have shown that collecting water signal may be used as a reference to correct the line-shape distortion caused by eddy currents, as an internal reference for absolute data quantification [8], or as an indication of the normal mammary tissue in breast cancer [9]. Therefore, post-processing techniques, based on signal-processing methods, might be considered as a good alternative to the pre-processing methods [10]–[13]. Several MRS post-processing technique methods have been proposed [14]–[16]. An example is the well-known Hankel-Lanczos Singular Value Decomposition (HLSVD) method [16] and the Hankel Lanczos squares Singular Values Decomposition with Partial Re-Orthogonalization (HLSVD-PRO) [17], [18]. The HLSVD-based methods decompose the unsuppressed residual water MRS spectrum into a set of exponentially decaying components, and select those with frequencies close to the frequency of water to reconstruct the water resonance. The method has several modifications to achieve better performance [19]–[21]. Other types of MRS water suppression methods include Gabor transform [22], Wavelet transform [23]–[25], Fourier-based method which uses a convolution difference of the time-domain to remove the water peak [26], and FIR based filters (MP-FIR) [27]. Optimization-based techniques have also been introduced to remove the water peak in MRS spectra. Such methods include Advanced Method for Accurate, Robust, and Efficient Spectral fitting (AMARES) [28], the Automated Quantization of Short Echo time MRS spectra (AQSES) [29] and the semi-parametric approach using regularization [30].

Despite the efforts in developing efficient water suppression post-processing methods, there are still several challenges to be addressed. For instance, the shape of the estimated water line may easily deviate from the theoretical Lorentzian model, which leads to non-efficient water removal. In addition, the low SNR of the output signal, once the water line is removed, may affect data quantification. To overcome these challenges, this paper proposes a new water suppression algorithm, based on the squared eigenfunctions associated with the negative eigenvalues of the Schrödinger operator. These eigenfunctions have been introduced in [31], for signal reconstruction and analysis, have been successfully used for the analysis of arterial blood pressure signal [32] as well as MRS denoising [33]. We refer to this method as SCSA for Semi Classical Signal Analysis (SCSA). The squared eigenfunctions of the Schrödinger operator have very interesting properties, suggesting their use for the analysis of pulse-shaped signals, as illustrated in [33]. This paper extends the usage of the SCSA method to water suppression in ^{1}H-MRS spectroscopy. The proposed algorithm consists of three steps: first, the water peak is estimated by partially reconstructing the MRS spectrum, using a minimum number of eigenfunctions. This step uses an iterative optimization problem to find the optimal choice of the number of eigenfunctions. Second, the eigenfunctions belonging to the water peak are selected, while those representing the metabolic peaks are discarded. Third, the subtraction of the estimated water peak from the input MRS spectrum provides the suppressed water MRS spectrum.

This paper is organized as follows: In section II, the proposed SCSA method for water suppression is introduced, and generation of simulated data, as well as, acquisition of *in vitro*, and *in vivo* MRS data are described. In section III, the SCSA results are presented, and discussed in section IV. Section V is devoted to the conclusion.

II. METHODS & MATERIALS

A. SIGNAL ANALYSIS USING THE SCHRÖDINGER OPERATOR

The use of the eigenfunctions of the Schrödinger operator for signal decomposition and representation has been introduced in [31] and [34] where it has been proven that a real positive input signal $y(f)$, that represents the real part of the MRS spectrum, can be approximated by $y_{h,\gamma}(f)$ given in the following form:

$$y_{h,\gamma}(f) = \left(\frac{h}{L_\gamma^{cl}} \sum_{n=1}^{N_h} (-\lambda_{nh})^\gamma \ \psi_{nh}^2(f) \right)^{\frac{2}{1+2\gamma}}, \tag{1}$$

where h and $\gamma \in \mathbb{R}_+^*$, λ_{nh} and $\psi_{nh}(f)$, for $n = 1, \cdots, N_h$, refer to the negative eigenvalues, with $\lambda_{1h} < \cdots < \lambda_{N_h h} < 0$, and their associated L^2-normalized eigenfunctions, respectively, of the semi-classical Schrödinger operator $H(y)$ defined as follows:

$$H(y) = -h^2 \frac{d^2}{df^2} - y, \tag{2}$$

with,

$$H(y)\,\psi(f) = \lambda\,.\psi(f), \tag{3}$$

where $L_\gamma^{cl} = \frac{1}{2^2\pi} \frac{\Gamma(\gamma+1)}{\Gamma(\gamma+2)}$ is the universal semi-classical constant, where Γ refers to the standard Gamma function.

The equation (1) provides an exact reconstruction of the signal when h converges to zero. This was the reason for calling this method the semi-classical signal analysis or SCSA where h is called the semi-classical parameter. Moreover, when h decreases, the number of eigenvalues increases and the reconstruction improves, as explained in [31]. The effect of the parameter γ has also been discussed in [34]. In this paper, we fix $\gamma = \frac{1}{2}$ and the equation becomes:

$$y_h(f) = 4h \sum_{n=1}^{N_h} \phi_{nh}(f) \tag{4}$$

where the spectral components $\phi_{nh}(f)$ are defined as follows:

$$\phi_{nh}(f) = \kappa_{nh}\ \psi_{nh}^2(f) \tag{5}$$

where $\kappa_{nh} = \sqrt{(-\lambda_{nh})}$.

The algorithm of the SCSA method for signal reconstruction has been reported in [31] and is given by:

Algorithm 1 The SCSA Reconstruction Algorithm

Input: MRS spectrum $y(f)$, h, γ.
Output: Reconstructed signal $y_h(f)$

Step 1: Discretization of the Schrödinger operator (eq. 2).
Step 2: Solving the eigenvalue problem.
Step 3: Selection of the negative eigenvalues and their associated L^2-normalized eigenfunctions.
Step 4: Reconstruction of the output signal $y_h(f)$ (eq. 4).

B. THE SCSA METHOD FOR PULSE-SHAPED SIGNAL RECONSTRUCTION

The SCSA is efficient in dealing with pulse-shaped signals, due to the nature of the squared eigenfunctions of the Schrödinger operator. It is known that the first squared eigenfunctions of the Schrödinger operator is localized at the maximum of the signal (i.e., the water peak in MRS spectrum) [33]. Moreover, as h decreases, the eigenfunction oscillations increase and their amplitudes decrease (for the n^{th} eigenfunction, the number of oscillations is given by $n+1$), as illustrated in figure 1. These first eigenfunctions have some interesting properties: they are very well localized around the most significant peaks in the MRS spectrum, and are model independent with no symmetric condition. This indicates that the SCSA is a suitable method for pulse-shaped signals. Because of the multi-peak nature of the MRS spectra, the SCSA is well-adapted for their analysis. However, two important challenges have to be addressed [31]. The first challenge is the significant difference in amplitude between the water peak and the metabolic peaks. The second challenge is the insufficient number of data points representing the MRS spectrum. Indeed for high amplitude signals (e.g., water peak), the required number of eigenfunctions for signal reconstruction is very large. This number cannot be reached as it is limited by the size of the discrete Laplacian, which depends on the number of data points. Therefore, the SCSA algorithm has to be adapted to overcome these limitations. Specifically, the proposed SCSA based algorithm removes the water peak from the MRS spectrum in three steps : first, it uses the eigenfunctions that dominantly reconstruct the water peak and which have a negligible contribution to the reconstruction of the metabolites. Secondly, it refines the reconstructed water peak by removing the eigenfunctions that are localized in the metabolites bandwidth. Finally, it subtracts the estimated water peak from the input spectrum to provide the water-suppressed MRS spectrum. The flowchart of the proposed method is shown in figure 2.

C. WATER PEAK ESTIMATION AND SUPPRESSION

The SCSA makes use of the large water peak property for its reconstruction with a small number of eigenfunctions due to the localization of its eigenfunctions (see figure 1). The water peak approximation is achieved in three steps:

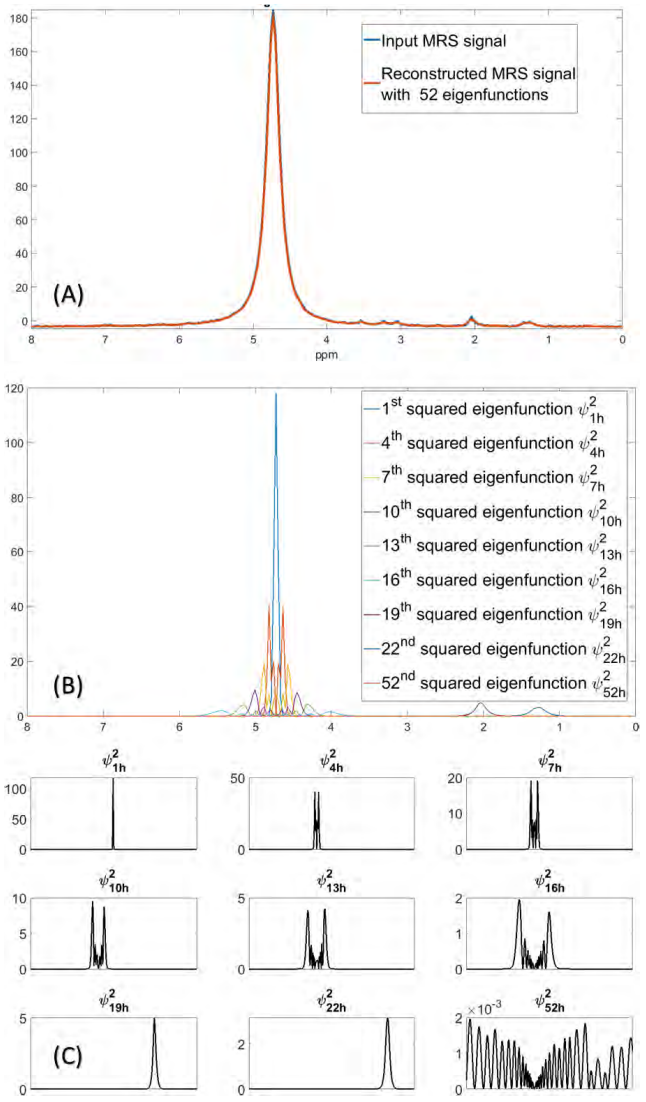

FIGURE 1. Example of spectral components $\phi_{nh}(f)$: (A) the input and reconstructed MRS spectrum using $h = 4.73$. (B) Selected eigenfunctions showing their localization property. (C) Illustration of the resemblance between the shape of these squared eigenfunctions and the profile of the input MRS peaks.

1) WATER PEAK RECONSTRUCTION

The SCSA is used to reconstruct the input MRS spectra using the set of N_{wp} eigenfunctions. However, only the first eigenfunctions will contribute mostly to the water peak reconstruction. The water peak can be reconstructed using a small eigenfunctions N_{wp}, such that $N_{wp} \simeq \frac{N}{140}$ which represents almost 0.8% of the length N of the input spectra based on the conducted experiment and dataset. Therefore, the optimal value of h, referred to as h_{wp}, should be determined in order to decompose the MRS spectrum into this determined set

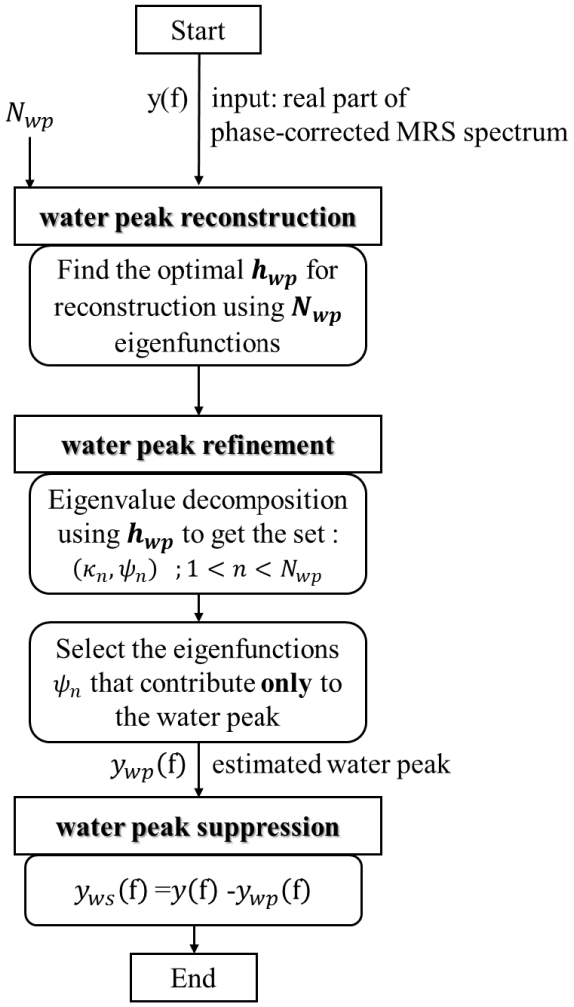

FIGURE 2. The flowchart of the proposed water suppression method.

Algorithm 2 Water Peak Estimation

Input :
y: input MRS spectrum
N_{wp}: Desired number of eigenfunctions

Output: y_{wp}: Estimated water peak

◇ *Reconstruct* y *using* N_{wp} *eigenfunctions*
$f_{water} \Leftarrow [-50Hz, 50Hz]$
$h_{wp}, N_{wp} \Leftarrow SCSA\_Nh(y, N_{wp})$
$\kappa, \psi = SCSA(y, h_{wp})$

◇ *Select eigenfunctions contributing to the water peak*
for $n \Leftarrow 1 \rightarrow N_{wp}$ **do**
  if $max(\psi_n) \in f_{water}$ **then**
    $S(n) \Leftarrow 1$ selected eigenfunction
  end
end

◇ *Subtract the water peak from the MRS spectra*
$$y_{wp}(f) = 4\, h_{wp} \sum_{n=1}^{N_{wp}} S(n)\, \kappa_{nh}\, \psi_{nh}^2(f)$$

return $y_{wp}(f)$

---

function $h_{wp}, N_h = SCSA\_Nh(y, N_{wp})$ $h \Leftarrow max(y)$,
$\gamma \Leftarrow \frac{1}{2}$. $(y_{out}, N_h) = SCSA(y, h)$
while $\|N_h - N_{wp}\| \neq 0$ **do**
  $h = h * \left(\frac{N_h}{N_{wp}}\right)$ $(y_{out}, N_h) = SCSA(y, h, \gamma)$
end
$h_{wp} = h$
return h_{wp}, N_h

of eigenfunctions. The optimal value of h_{wp} is found using an iterative optimization process as shown in the algorithm 2.

Each one of the desired computed N_{wp} eigenfunctions contributes to the reconstruction of some specific details within the MRS spectrum.

2) WATER PEAK REFINEMENT

In this part, the eigenfunctions that contribute mostly to the water peak are selected to refine the estimated water peak $y_{wp}(f)$ given by:

$$y_{wp}(f) = 4h_{wp} \sum_{n=1}^{N_{wp}} S(n)\, \kappa_{nh}\, \psi_{nh}^2(f) \tag{6}$$

where $S(n)$ is the selection function defined by:

$$S(n) = \begin{cases} 1, & \text{if } \psi_{nh}(f) \text{ is selected} \\ 0, & \text{elsewhere} \end{cases} \tag{7}$$

The water peak reconstruction and the eigenfunction selection are described in Algorithm 2 and illustrated in Figure 3.

3) WATER SUPPRESSION

Once the water peak is removed, the suppressed water MRS spectrum $y_{ws}(f)$ is given by:

$$y_{ws}(f) = y(f) - y_{wp}(f) \tag{8}$$

In some water suppression cases, the water residue is still large. This residue might affect the convergence of the used quantification method. To solve this problem, the water residue is further attenuated using the SCSA recursively, as shown in Figure 4. The algorithm used for water residue reduction is described in Algorithm 3. The proposed SCSA based residual water suppression method will be tested on different simulated and real MRS datasets. The results are shown and discussed in the next sections.

D. MATERIALS AND DATASETS

1) SIMULATED DATA

Unsuppressed water spectroscopy data were simulated using a basis set from the ISMRM MRS Fitting Challenge 2016. This basis consisted of MRS spectra from

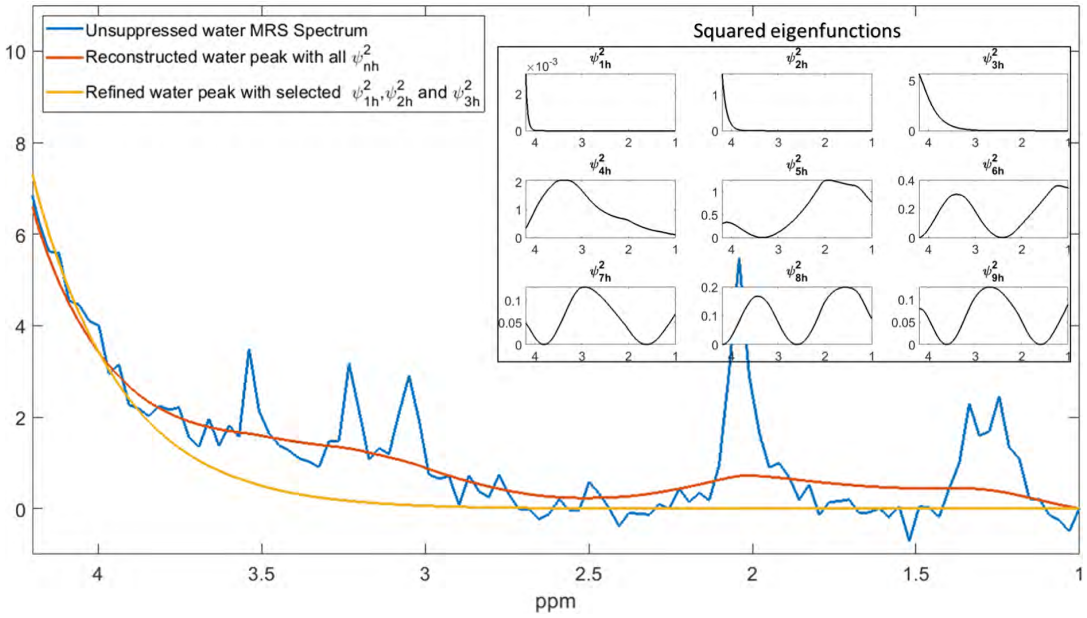

FIGURE 3. MRS water peak estimation using eigenfunction selection using $N_{wp} = 9$ eigenfunctions.

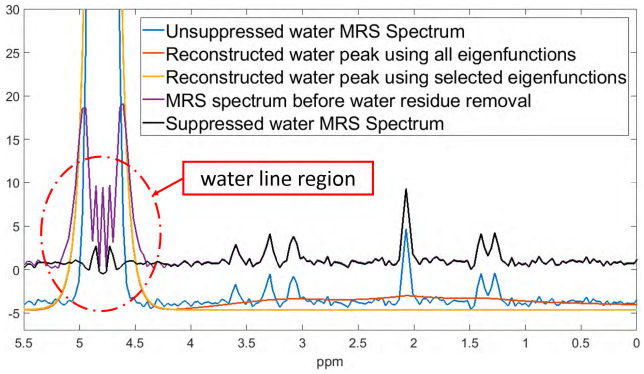

FIGURE 4. Example of water residue attenuation.

Algorithm 3 Water Residue Attenuation

Input :

y_{ws}: water suppressed MRS spectrum
L_{ws}: Number of loop used for attenuation
N_{wr}: The used number of eigenfunctions

Output:

y_{ws2}: MRS spectrum with attenuated water residue

$f_{water} \Leftarrow [-50Hz, 50Hz]$
$y \Leftarrow y_{ws}(f_{water})$

for $n \Leftarrow 1 \rightarrow L_{ws}$ **do**
  $y_{wr} \Leftarrow SCSA\_Nh(y, N_{wr})$
end

$y_{ws2} \Leftarrow y_{ws}\, y_{ws2}(f_{water}) \Leftarrow y_{wr}$
return $y_{ws2}(f_{water})$

Alanine (Ala), Aspartate (Ala), Choline (Cho), Creatine (Cr), γ-aminobutyric acid (GABA), Glutamate (Glu), Lactate (Lac), two lipids (Lip1 and Lip2), myo-Inositol (mI), N-Acetyl-Aspartate (NAA) and Taurine (Tau) metabolites. 100 MRS spectra consisting of the 12 metabolites above with different amplitudes at three different signal-to-noise ratio (SNR, defined as the ratio of the power of the signal to the power of the noise) values, namely 5dB, 10dB, and 20dB were generated first. The following acquisition parameters were used for data simulation for a 3 Tesla field strength (Larmor frequency = 123.2 MHz). Sequence: PRESS, $TE = 30$ ms, $TE1 = 11$ ms, $TE2 = 19$ ms, Spectral width = 4000 Hz, Number of points = 2048, tissue content: Gray Matter (GM) = 60%, White Matter (WM) = 40%, Water content: GM = 0.78 g/ml, WM = 0.65 g/ml, $T2$ of water: GM = 110 ms, WM = 80 ms, $T2$ of metabolites = 160 ms. Next, the water signal, simulated separately using the same dataset above, was then multiplied by the $e^{d_k t^2}$ factor to imitate the baseline distortion. Note that d_k was modeled as a uniformly distributed random variable between 0 and 0.005. Finally, the distorted water line was added to the noisy metabolite signals to generate the unsuppressed water MRS dataset.

2) *IN VITRO* DATA

In vitro water unsuppressed data was collected from a 3T Siemens whole body scanner using $TE/TR = 30/2000$ ms, 1024 points, a bandwidth of 1250 Hz, $N_{avg} = 8$, and $20 \times 20 \times 20$ mm^3 voxel size from a spherical water solution phantom containing NAA and lactate with known concentrations of 1 mM each. SCSA and HLSVD-PRO methods were applied on the water unsuppressed data. The water line was

calculated from the unsuppressed water data and used as an internal reference to estimate the absolute concentrations of the metabolites. The absolute concentrations of the metabolites were estimated using the following equation:

$$C_{metabolite} = C_{water} \times \left(\frac{2}{np}\right) \times \left(\frac{A_{metabolite}}{A_{water}}\right) \times \frac{exp\left(\frac{TE}{T2_{metabolite}}\right)}{exp\left(\frac{TE}{T2_{water}}\right)} \times \frac{\left\{1 - exp\left(\frac{-TR}{T1_{water}}\right)\right\}}{\left\{1 - exp\left(\frac{-TR}{T1_{metabolite}}\right)\right\}} \quad (9)$$

The variable $C_{metabolite}$ is the metabolite concentration (mM), C_{water} is the water concentration used as an internal reference (110 M) [35], [36], $A_{metabolite}$ is the area of the metabolite peak, A_{water} is the area of the water peak calculated from the unsuppressed water data, np is the number of protons of a metabolite, and $T1_{metabolite}$, $T2_{metabolite}$, $T1_{water}$, $T2_{water}$ are the relaxation times of metabolites and water [35]–[40].

3) *IN VIVO* DATA

In vivo data was collected from a 3T Siemens whole body scanner with a total gradient strength of 45 mT/m and a nominal slew rate of 200 mT/m/s. A 32-channel receive head coil was used for data acquisition.

In vivo CHESS [3] water suppressed 16×16 MRSI data was collected from 10 healthy volunteers using the Chemical Shift Imaging (CSI) sequence, using the following parameters: $TE = 35\ ms$, $TR = 2000\ ms$, Field of view (FOV): $100 \times 100 mm^2$, $BW = 2000\ Hz$, $N_{full} = 512$, $N_{avg} = 2$. Manual and automatic shimming were performed to maintain the full-width half-maximum (FWHM) of the water peak around 20 Hz. From the MRSI grid of each volunteer, four voxels were selected (two close to the center of FOV and two near the edge of FOV). Water residual removal was performed on the selected voxels using both SCSA and HLSVD-PRO methods. Two single voxel *in vivo* CHESS water suppressed data (frontal lobe region) were collected with the same acquisition parameters as the *in vitro* data. The CHESS water suppression factor was varied to collect one spectrum with the best water suppression (minimal water residue) and a second spectrum with poor water suppression (large water residue). SCSA and HLSVD-PRO methods were applied on the spectrum with large water residue, and compared to the one with minimal water residue.

4) DATA PROCESSING AND QUANTIFICATION

All experimental data analysis was performed using Matlab (MathWorks, USA). Water suppression was performed using both SCSA and HLSVD-PRO [17], [18] algorithms for comparison purposes. All spectra were phase-corrected with respect to the water peak before suppression. The model order of HLSVD-PRO was set to 10. This model order was chosen since it provided the optimum suppression considering all the collected data [41]. For the *in vivo* MRSI data, the NAA at 2.02 ppm, Cho at 3.2 ppm, total Creatine (tCr) at 3.03 ppm, mI at 3.55 ppm, and tCr at 3.9 ppm peaks were fitted to a Lorentzian model using a quantification approach which iteratively performs baseline estimation first, followed by the peak quantification procedure using AMARES [28], [42]. This approach has been previously shown to yield better quantification results as compared to the single pass optimization method that models baseline and metabolite signals together [43]. We also run Cramér Rao bounds criteria on the quantified peaks to check on the quality of water suppression. The average Cramér-Rao bounds in percentage of the quantified amplitude of the metabolite peaks along with the standard deviations, are measured for all the signals. Zero-filling with a factor of 2 is also performed to improve the resolution of the spectra.

TABLE 1. Absolute quantification *in vitro* results in mM for NAA and Lac peaks after water suppression using SCSA and the HLSVD-PRO and their comparison to the expected values.

	NAA (mM)	Lac (mM)
Expected	**1.0**	**1.0**
SCSA	**0.95**	**0.97**
HLSVD-PRO	**0.95**	**0.96**

III. RESULTS

To investigate the robustness of the methods, we have analyzed the results in term of residual error and difference in variance for simulated, *in vitro*, and *in vivo* MRS(I) data, respectively. Furthermore, we have assessed the water suppression quality of both methods using the average Cramér-Rao bounds [44], which are generally used in *in vivo* studies to assess the reliability of data quantification.

A. RESULTS WITH SIMULATED DATA

In Figure 5, the boxplot of the residual error between the water-suppressed signals using SCSA (Figure 6c) and HLSVD-PRO (Figure 6d) and the metabolite signals without water line (Figure 6a) at three different noise levels are displayed. Both methods provide comparable performance in terms of the residual error values. However, the boxplot in Figure 5 indicates that the SCSA has a lower median error compared to the HLSVD-PRO method for a lower noise level (SNR = 10 dB and 20 dB) but the error range is higher compared to HLSVD-PRO. The performance of SCSA also slightly dropped for a higher noise level (SNR = 5 dB).

B. IN VITRO RESULTS

The *in vitro* spectrum was processed using SCSA and HLSVD-PRO. The results are shown in Figure 7. The absolute quantification results using both methods are reported in Table 1. Both methods provided accurate results when compared to the expected ones.

C. IN VIVO RESULTS

To further test the performance of the algorithms, the selected 40 *in vivo* signals from the ten volunteers, as described

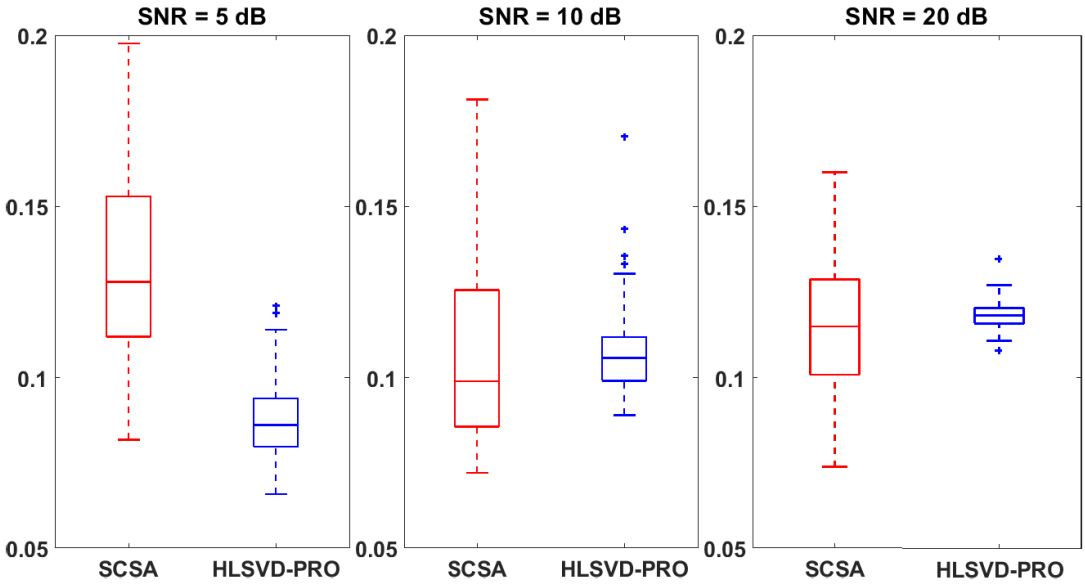

FIGURE 5. Boxplot of the residual errors after water suppression using the SCSA (red) and HLSVD-PRO (blue) methods on 100 simulated MRS spectra at three different noise realizations (SNR = 5 dB, 10 dB, 20 dB). The error is calculated as the l_2-norm of the difference between the water suppressed signal and the original water free signal (with noise).

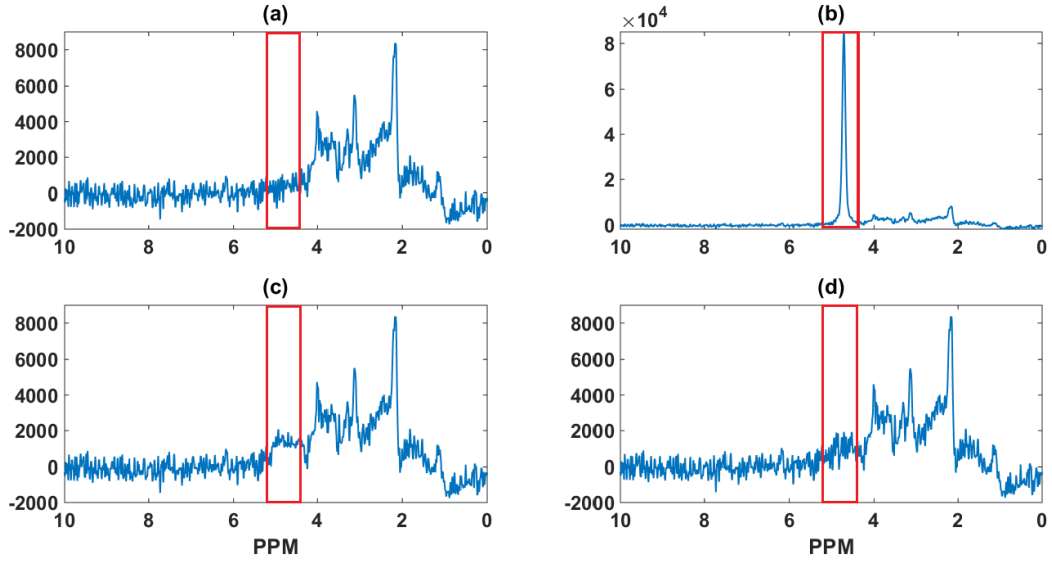

FIGURE 6. (a) Absorption spectrum of a simulated MRS spectrum without water. (b) Absorption spectrum of a simulated MRS spectrum with an added water peak. Absorption spectrum of the water suppressed signal using (c) SCSA and (d) HLSVD-PRO. Red vertical boxes in all the sub figures indicate the water region.

in the Methods section, were processed using SCSA and HLSVD-PRO. Both methods performed efficient water residue removal, in most cases. Since no ground truth was available for *in vivo* data to assess the quality of water suppression, the performance of the methods was assessed by calculating the difference between the variance of the suppressed water region (4.2 to 5.2 ppm) and the variance of the noise region located at the outer edges of the spectrum.

The boxplot of variance difference of the selected 40 *in vivo* MRS spectra for both methods is shown in Figure 8. One can see that SCSA performs comparably to the HLSVD-PRO in suppressing the water residue. Computed NAA/Cr and Cho/Cr ratios of the 40 *in vivo* MRS spectra for the SCSA and HLSVD-PRO methods are displayed in the boxplot in Figure 9. Figure 10 shows the spectra of the results obtained using *in vivo* MRSI data from one of the volunteers. Both methods provide comparable quantification results since the metabolites ratios are in agreement with the literature [45].

The Cramér-Rao bounds of the quantified metabolite peak amplitudes are reported in Table 2. Although both methods provide similar results, higher Cramér-Rao bounds are observed with HLSVD-PRO than the SCSA method.

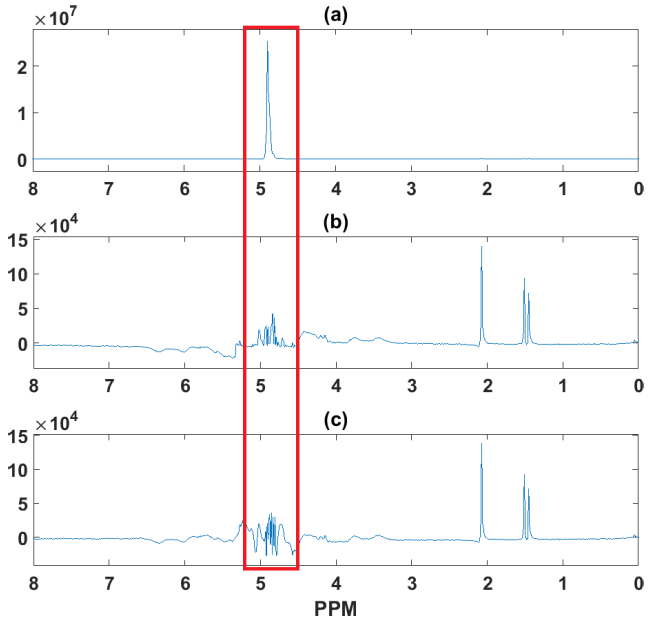

FIGURE 7. (a) Absorption spectra (phase-corrected) of water unsuppressed *in vitro* data, (b) showing the water suppressed *in vitro* data using SCSA and (c) showing the water suppressed *in vitro* data using HLSVD-PRO. Red vertical boxes in all the sub figures indicate the water region.

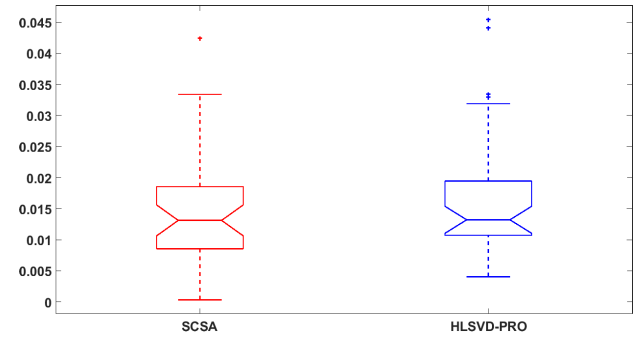

FIGURE 8. Boxplots of error after residual water suppression using SCSA (red) and HLSVD-PRO (blue) on *in vivo* MRSI data. The error is calculated as the difference between the variance of the suppressed water region and the variance of noise region.

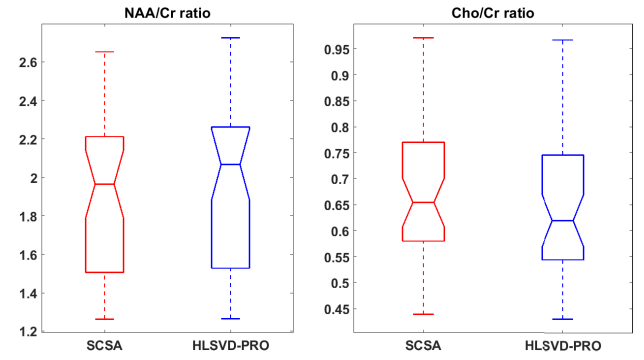

FIGURE 9. *In vivo* quantification results given as metabolite ratios after residual water removal using SCSA (red) and HLSVD-PRO (blue).

The performance of the SCSA method (Figure 11c) and HLSVD-PRO method (Figure 11d) applied on the single voxel spectroscopy data with large water residue

TABLE 2. Mean and standard deviation of Cramér-Rao bounds in % of quantified amplitudes for NAA, Cho, tCr (3.03 ppm), mI and tCr (3.9 ppm) metabolite peaks for the *in vivo* data.

	Mean		Standard deviation	
	SCSA	*HLSVD-PRO*	*SCSA*	*HLSVD-PRO*
NAA	2.46	2.60	1.20	1.15
Cho	2.40	2.56	1.60	1.30
tCr (3.03 ppm)	4.24	5.80	2.25	1.20
mI	14.70	25.60	9.76	10.80
tCr (3.9 ppm)	13.40	17.12	5.38	8.10

TABLE 3. Average residual error in the metabolite and downfield segment after water suppression using SCSA and HLSVD-PRO with respect to a CHESS water suppression in single voxel spectroscopy *in vivo* data.

	Residual error (metabolite segment)	Residual error (Downfield)
SCSA	**0.02**	**0.05**
HLSVD-PRO	**0.02**	**0.03**

(Figure 11b) were compared to those with minimal water residue (Figure 11a) in terms of average residual error in the metabolite region (1 PPM - 4.2 PPM) and the downfield region ($\geq$5.3 PPM). Both methods provided similar results with no baseline distortion as reported in Table 3 and shown in Figure 11.

IV. DISCUSSION

We have developed a model free approach to perform water suppression for MRS spectra using SCSA. In the simulation results, water suppressed signals using SCSA (Figure 6c) and HLSVD-PRO (Figure 6d) by applying water suppression on the simulated MRS spectrum with an added water peak (Figure 6b) were comparable in terms of residual error with respect to the simulated reference metabolite signal without water line (Figure 6a). From the box plots in Figure 5 obtained using the spectra from Figure 6 at three different SNR levels, we observed very low residual error values for both SCSA and HLSVD at high SNR values. The differences in median value and error range were not found to be significant between the two methods. However at low SNR value of 5 dB, HLSVD provided a better water suppression with less residual error than SCSA. But, the residual errors obtained using both techniques were very low and not significant from the box plot in Figure 5 and hence they are comparable. For single voxel MRS data (*in vitro* and *in vivo*), both SCSA and HLSVD-PRO methods achieve efficient water suppression without affecting the peaks of interest (Figure 7 and Table 1, Figure 11 and Table 3). However, the situation is more challenging in the case of MRSI, where the data generally suffers from low SNR, field in-homogeneity, and lower water suppression efficiency, causing baseline distortion and peak shape deformation. Still, the SCSA was capable to provide comparable results to HLSVD as demonstrated by Figures 8-10.

Since SCSA is a model-free approach, it adapts to any given water residue shape whereas other suppression techniques rely on a predefined model to estimate and remove

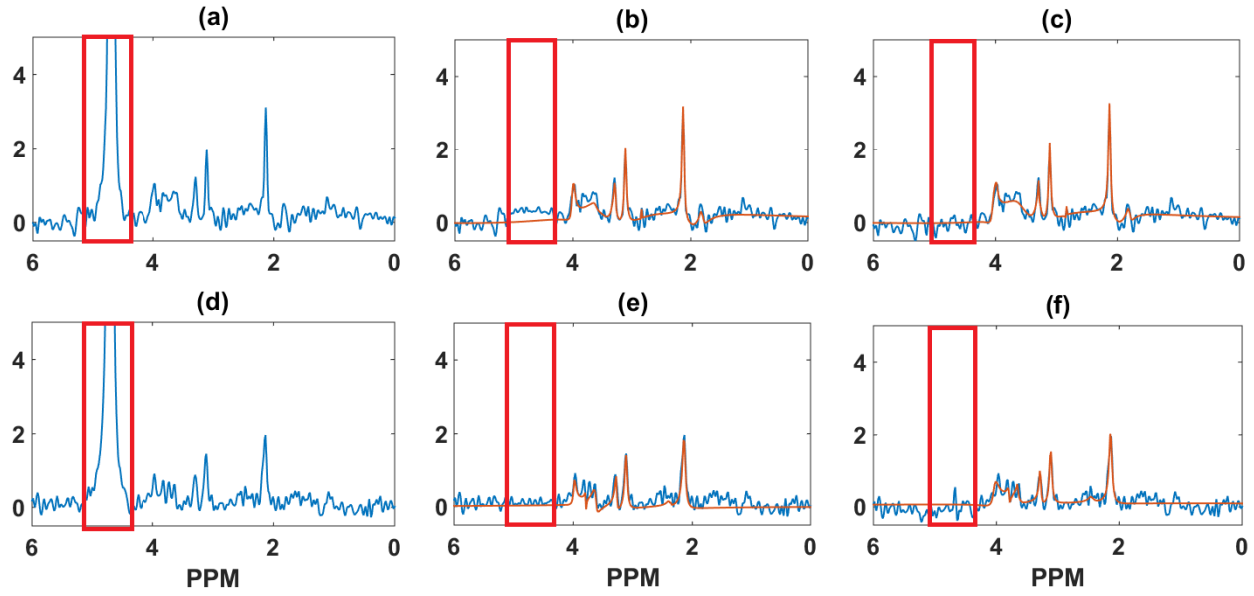

FIGURE 10. (a) Phase corrected absorption spectrum with large water residue *in vivo* of a voxel selected from the center of FOV of MRSI data of one volunteer. The SCSA result on the spectrum of Fig (a) is shown in blue in Fig (b), and the fitting result is shown in red. Similarly, the HLSVD-PRO result is shown in blue in Fig (c) and the corresponding fitting result is shown in red. (d) Phase corrected absorption spectrum with large water residue of a voxel selected from the edge of FOV of the same volunteer. The SCSA result on the spectrum of Fig (d) is shown in blue in Fig (e), and the fitting result is shown in red. Similarly, the HLSVD-PRO result is shown in blue in Fig (f) and the corresponding fitting result is shown in red. Red vertical boxes in all the sub figures indicate the water region.

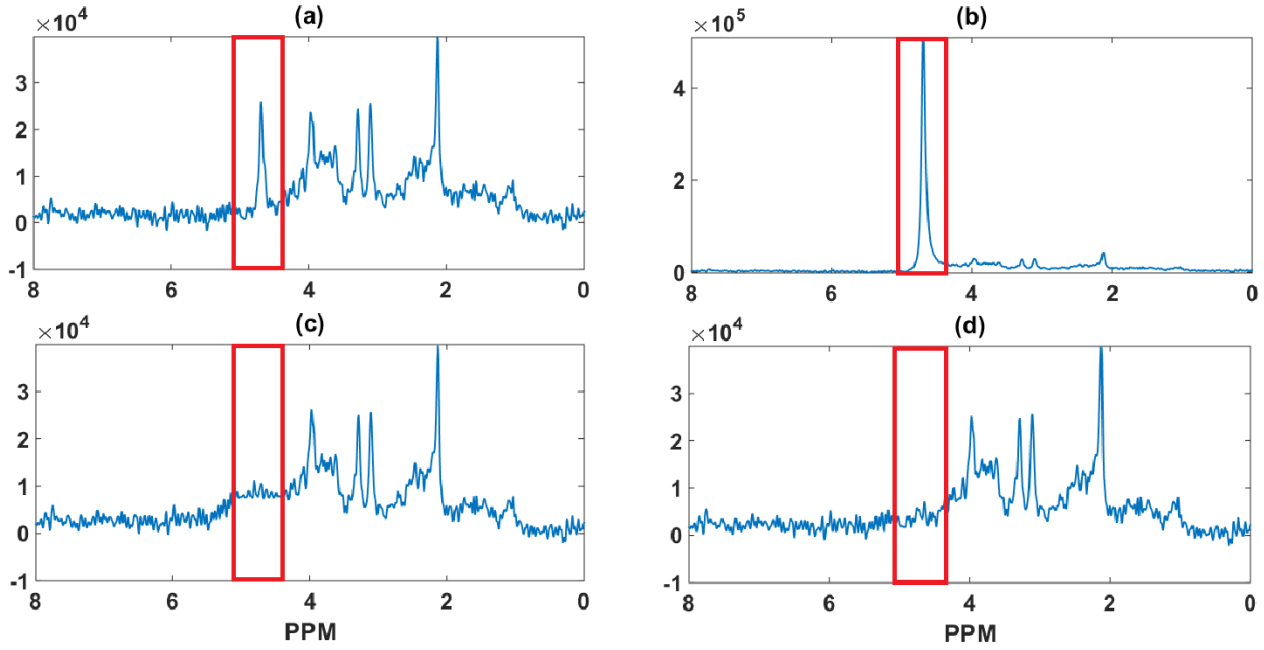

FIGURE 11. (a) Single voxel *in vivo* phase-corrected absorption spectrum with minimal water residue after CHESS, (b) single voxel *in vivo* phase-corrected absorption spectrum with large water residue after CHESS, (c) SCSA result on the spectrum of Fig (b), and (d) HLSVD-PRO result on the spectrum of Fig (b). Red vertical boxes in all the sub figures indicate the water region.

the water line (e.g: Lorentzian model used in HLSVD). Due to the decomposition of the input spectrum into a set of eigenfunctions, the proposed method selects the eigenfunctions belonging to the water residue signal only and discard those representing noise and data artifacts. The eddy current effect will appear on the collected spectra as baseline distortion or field inhomogeneity effect. Their effect on MRSI data was reduced using (e.g.: QUALITY [46], ECC [47]) methods prior to data analysis. The SCSA method was insensitive to the effect of eddy currents.

The SCSA processes the real part of the phase corrected MRS(I) data in the frequency domain. This is in agreement, with the MRS users, where only the real part of the phase corrected MRS(I) data is used for data quantification. Both zero and first order phase corrections are performed prior to the water suppression. This is essential, since it helps aligning the water peak properly to a pulse-shaped signal form prior to SCSA processing. However, to take into consideration the full MRS information, considering the complex MRS spectrum is currently under investigations. This will improve the outcome and bypass few pre-processing steps such as phase correction step. The preliminary results obtained so far on the complex MRS spectrum are encouraging.

We also refined the SCSA method for a more efficient water suppression while preserving the metabolite signals. This was achieved by carefully selecting the eigenfunctions belonging to water residue and discarding those representing the peaks of interest. The number of required eigenfunctions N_{wp} used to represent the water peak depends on the total number of samples and the maximum amplitude of the MRS spectrum. In our tests, we choose N_{wp} to be $N_{wp} = N/140$.

V. CONCLUSION

Suppression of the residual water signal from proton MRS data in the human brain is a prerequisite for an accurate quantification of brain metabolites. A novel and efficient post-processing water suppression technique based on the squared eigenfunctions of the Schrödinger operator has been proposed. The method efficiently extracts the water peak (or residue) from the MRS unsuppressed water spectrum without altering the small metabolite resonances. The real part of the input spectrum was decomposed into a set of eigenfunctions of the Schrödinger operator first. Those contributing mostly to the water peak (or residue) were subtracted from the original data using a model-independent approach, leading to a water free spectrum (with complicated or unknown lineshapes), without attenuating the remaining small peaks in the spectrum. This was confirmed by the results obtained from simulated, *in vitro* and *in vivo* data. Furthermore, the proposed method performs comparably to the HLSVD-PRO in preserving metabolite information after residual water suppression, while efficiently addressing the baseline distortion caused by the water residue as demonstrated with the help of simulated, *in vitro* and *in vivo* data. SCSA is a novel method which performs as good as the established standard HLSVD technique in term of residual water suppression. In addition, the method has been shown to be efficient in MRS data denoising. These results have been obtained while processing the real part of the MRS data only. However, to fully explore the potential of this method, Future work will focus on extending the SCSA to complex MRS spectra.

ACKNOWLEDGMENT

The authors would like to thank Dr. Sabine Van Huffel from the University of Leuven for the use of the HLSVD software, Ms. Patricia Clement and Ghent Institute for Functional and Metabolic Imaging (GIfMI) team for their help in the *in vivo* data acquisition.

REFERENCES

[1] B. L. Miller, "A review of chemical issues in ^{1}H NMR spectroscopy: *N*-acetyl-l-aspartate, creatine and choline," *NMR Biomed.*, vol. 4, no. 2, pp. 47–52, 1991.

[2] G. Öz *et al.*, "Clinical proton MR spectroscopy in central nervous system disorders," *Radiology*, vol. 270, no. 3, pp. 658–679, 2014.

[3] A. Haase, J. Frahm, W. Hanicke, and D. Matthaei, "^{1}H NMR chemical shift selective (CHESS) imaging," *Phys. Med. Biol.*, vol. 30, no. 4, p. 341, 1985.

[4] R. J. Ogg, R. B. Kingsley, and J. S. Taylor, "WET, a T_1- and B_1-insensitive water-suppression method for *in vivo* localized 1H NMR spectroscopy," *J. Magn. Reson. B*, vol. 104, no. 1, pp. 1–10, May 1994.

[5] I. Tkáč, Z. Starčuk, I.-Y. Choi, and R. Gruetter, "*In vivo* ^{1}H NMR spectroscopy of rat brain at 1 ms echo time," *Magn. Reson. Med.*, vol. 41, no. 4, pp. 649–656, 1999.

[6] M. A. Smith, J. Gillen, M. T. McMahon, P. B. Barker, and X. Golay, "Simultaneous water and lipid suppression for in vivo brain spectroscopy in humans," *Magn. Reson. Med.*, vol. 54, no. 3, pp. 691–696, Sep. 2005.

[7] J.-M. Lin *et al.*, "Quantification of non–water-suppressed MR spectra with correction for motion-induced signal reduction," *Magn. Reson. Med.*, vol. 62, no. 6, pp. 1394–1403, 2009.

[8] Y. Zhang, S. Marenco, and J. Shen, "Correction of frequency and phase variations induced by eddy currents in localized spectroscopy with multiple echo times," *Magn. Reson. Med.*, vol. 58, no. 1, pp. 174–178, 2007.

[9] D. Belkic and K. Belkic, *Signal Processing in Magnetic Resonance Spectroscopy With Biomedical Applications*. Boca Raton, FL, USA: CRC Press, 2010.

[10] Y. Le Fur and P. J. Cozzone, "FID modulus: A simple and efficient technique to phase and align MR spectra," *Magn. Reson. Mater. Phys., Biol. Med.*, vol. 27, no. 2, pp. 131–148, 2014.

[11] A. Hock *et al.*, "Non-water-suppressed proton MR spectroscopy improves spectral quality in the human spinal cord," *Magn. Reson. Med.*, vol. 69, no. 5, pp. 1253–1260, 2013.

[12] Z. Dong, W. Dreher, and D. Leibfritz, "Toward quantitative short-echo-time *in vivo* proton MR spectroscopy without water suppression," *Magn. Reson. Med.*, vol. 55, no. 6, pp. 1441–1446, Jun. 2006.

[13] J.-H. Chen *et al.*, "Water suppression without signal loss in HR-MAS ^{1}H NMR of cells and tissues," *J. Magn. Reson.*, vol. 171, no. 1, pp. 143–150, Nov. 2004.

[14] Y.-Y. Lin, P. Hodgkinson, M. Ernst, and A. Pines, "A novel detection–estimation scheme for noisy NMR signals: Applications to delayed acquisition data," *J. Magn. Reson.*, vol. 128, no. 1, pp. 30–41, Sep. 1997.

[15] D. Belkić and K. Belkić, "The fast Padé transform in magnetic resonance spectroscopy for potential improvements in early cancer diagnostics," *Phys. Med. Biol.*, vol. 50, no. 18, p. 4385, 2005.

[16] W. W. F. Pijnappel, A. van den Boogaart, R. de Beer, and D. van Ormondt, "SVD-based quantification of magnetic resonance signals," *J. Magn. Reson.*, vol. 97, no. 1, pp. 122–134, Mar. 1992.

[17] T. Laudadio, N. Mastronardi, L. Vanhamme, P. Van Hecke, and S. Van Huffel, "Improved Lanczos algorithms for blackbox MRS data quantitation," *J. Magn. Reson.*, vol. 157, no. 2, pp. 292–297, Aug. 2002.

[18] H. Barkhuijsen, R. de Beer, and D. van Ormondt, "Improved algorithm for noniterative time-domain model fitting to exponentially damped magnetic resonance signals," *J. Magn. Reson.*, vol. 73, no. 3, pp. 553–557, Jul. 1987. [Online]. Available: http://www.sciencedirect.com/science/article/pii/0022236487900230

[19] D. S. Kim, H. K. Lee, Y. D. Won, D. G. Kim, Y. W. Lee, and H. S. Won, "NMR solvent peak suppression by piecewise polynomial truncated singular value decomposition methods," *Bull. Korean Chem. Soc.*, vol. 24, no. 7, pp. 967–970, 2003.

[20] R. Romano, A. Motta, S. Camassa, C. Pagano, M. T. Santini, and P. L. Indovina, "A new time-domain frequency-selective quantification algorithm," *J. Magn. Reson.*, vol. 155, no. 2, pp. 226–235, Apr. 2002.

[21] E. Cabanes, S. Confort-Gouny, Y. Le Fur, G. Simond, and P. J. Cozzone, "Optimization of residual water signal removal by HLSVD on simulated short echo time proton MR spectra of the human brain," *J. Magn. Reson.*, vol. 150, no. 2, pp. 116–125, 2001.

[22] J.-P. Antoine, A. Coron, and J.-M. Dereppe, "Water peak suppression: Time-frequency vs time-scale approach," *J. Magn. Reson.*, vol. 144, no. 2, pp. 189–194, Jun. 2000.
[23] D. Barache, J.-P. Antoine, and J.-M. Dereppe, "The continuous wavelet transform, an analysis tool for NMR spectroscopy," *J. Magn. Reson.*, vol. 128, no. 1, pp. 1–11, Sep. 1997.
[24] H. Serrai, L. Senhadji, D. B. Clayton, C. Zuo, and R. E. Lenkinski, "Water modeled signal removal and data quantification in localized MR spectroscopy using a time-scale postacquistion method," *J. Magn. Reson.*, vol. 149, no. 1, pp. 45–51, Mar. 2001.
[25] U. L. Günther, C. Ludwig, and H. Rüterjans, "WAVEWAT—Improved solvent suppression in NMR spectra employing wavelet transforms," *J. Magn. Reson.*, vol. 156, no. 1, pp. 19–25, May 2002.
[26] D. Marion, M. Ikura, and A. Bax, "Improved solvent suppression in one- and two-dimensional NMR spectra by convolution of time-domain data," *J. Magn. Reson.*, vol. 84, no. 2, pp. 425–430, Sep. 1989.
[27] J.-B. Poullet, R. Pintelon, and S. van Huffel, "A new FIR filter technique for solvent suppression in MRS signals," *J. Magn. Reson.*, vol. 196, no. 1, pp. 61–73, Jan. 2009. [Online]. Available: http://www.sciencedirect.com/science/article/pii/S1090780708003339
[28] L. Vanhamme, A. van den Boogaart, and S. Van Huffel, "Improved method for accurate and efficient quantification of MRS data with use of prior knowledge," *J. Magn. Reson.*, vol. 129, no. 1, pp. 35–43, Nov. 1997.
[29] J.-B. Poullet *et al.*, "An automated quantitation of short echo time MRS spectra in an open source software environment: AQSES," *NMR Biomed.*, vol. 20, no. 5, pp. 493–504, Aug. 2007.
[30] C. Elster, F. Schubert, A. Link, M. Walzel, F. Seifert, and H. Rinneberg, "Quantitative magnetic resonance spectroscopy: Semi-parametric modeling and determination of uncertainties," *Magn. Reson. Med.*, vol. 53, no. 6, pp. 1288–1296, 2005.
[31] T.-M. Laleg-Kirati, E. Crépeau, and M. Sorine, "Semi-classical signal analysis," *Mathematics Control, Signals, Syst.*, vol. 25, no. 1, pp. 37–61, 2013.
[32] T.-M. Laleg, E. Crépeau, Y. Papelier, and M. Sorine, "Arterial blood pressure analysis based on scattering transform I," in *Proc. 29th Annu. Int. Conf. IEEE Eng. Med. Biol. Soc. (EMBS)*, Aug. 2007, pp. 5326–5329.
[33] T.-M. Laleg-Kirati, J. Zhang, E. Achten, and H. Serrai, "Spectral data de-noising using semi-classical signal analysis: Application to localized MRS," *NMR Biomed.*, vol. 29, no. 10, pp. 1477–1485, 2016.
[34] B. Helffer and T.-M. Laleg-Kirati, "On semi-classical questions related to signal analysis," *Asymptotic Anal.*, vol. 75, nos. 3–4, pp. 125–144, 2011. [Online]. Available: http://hdl.handle.net/10754/561951
[35] H. Serrai, D. B. Clayton, L. Senhadji, C. Zuo, and R. E. Lenkinski, "Localized proton spectroscopy without water suppression: Removal of gradient induced frequency modulations by modulus signal selection," *J. Magn. Reson.*, vol. 154, no. 1, pp. 53–59, Jan. 2002.
[36] M. Terpstra, W. B. High, Y. Luo, R. A. de Graaf, H. Merkle, and M. Garwood, "Relationships among lactate concentration, blood flow and histopathologic profiles in rat C6 glioma," *NMR Biomed.*, vol. 9, no. 5, pp. 185–194, Aug. 1996.
[37] T. Isobe *et al.*, "Quantification of cerebral metabolites in glioma patients with proton MR spectroscopy using T2 relaxation time correction," *Magn. Reson. Imag.*, vol. 20, no. 4, pp. 343–349, May 2002.
[38] T. Ernst, R. Kreis, and B. Ross, "Absolute quantitation of water and metabolites in the human brain. I. Compartments and water," *J. Magn. Reson. B*, vol. 102, no. 1, pp. 1–8, Aug. 1993. [Online]. Available: http://www.sciencedirect.com/science/article/pii/S1064186683710551
[39] A. Matsumura, T. Isobe, S. Takano, H. Kawamura, and I. Anno, "Non-invasive quantification of lactate by proton MR spectroscopy and its clinical applications," *Clin. Neurol. Neurosurgery*, vol. 107, no. 5, pp. 379–384, Aug. 2005.
[40] P. A. Bottomley, T. H. Foster, R. E. Argersinger, and L. M. Pfeifer, "A review of normal tissue hydrogen NMR relaxation times and relaxation mechanisms from 1–100 MHz: Dependence on tissue type, NMR frequency, temperature, species, excision, and age," *Med. Phys.*, vol. 11, no. 4, pp. 425–448, Aug. 1984.
[41] L. Vanhamme, R. D. Fierro, S. Van Huffel, and R. de Beer, "Fast removal of residual water in proton spectra," *J. Magn. Reson.*, vol. 132, no. 2, pp. 197–203, Jun. 1998.
[42] K. Young, B. J. Soher, and A. A. Maudsley, "Automated spectral analysis II: Application of wavelet shrinkage for characterization of non-parameterized signals," *Magn. Reson. Med.*, vol. 40, no. 6, pp. 816–821, Dec. 1998.
[43] B. J. Soher, K. Young, and A. A. Maudsley, "Representation of strong baseline contributions in ^{1}H MR spectra," *Magn. Reson. Med.*, vol. 45, no. 6, pp. 966–972, Jun. 2001.
[44] S. Cavassila, S. Deval, C. Huegen, D. van Ormondt, and D. Graveron-Demilly, "Cramér–Rao bounds: An evaluation tool for quantitation," *NMR Biomed.*, vol. 14, no. 4, pp. 278–283, Jun. 2001.
[45] Y. Safriel, M. Pol-Rodriguez, E. J. Novotny, D. L. Rothman, and R. K. Fulbright, "Reference values for long echo time MR spectroscopy in healthy adults.," *AJNR. Amer. J. Neuroradiol.*, vol. 26, no. 6, pp. 1439–1445, Jul. 2005.
[46] A. A. De Graaf, J. E. Van Dijk, and W. M. Bovée, "Quality: Quantification improvement by converting lineshapes to the Lorentzian type," *Magn. Reson. Med.*, vol. 13, no. 3, pp. 343–357, Mar. 1990.
[47] U. Klose, "*In vivo* proton spectroscopy in presence of eddy currents," *Magn. Reson. Med.*, vol. 14, no. 1, pp. 26–30, Apr. 1990.

ABDERRAZAK CHAHID received the B.Sc. degree in electrical engineering and power electronics from University Sultan Moulay Slimane, the M.Sc. degree in electrical engineering from the National School of Applied Sciences, Morocco, and the M.Sc. degree in embedded systems from the University of Lorraine, France. He is currently pursuing the Ph.D. degree with the Electrical Engineering Department, CEMSE Division, King Abdullah University of Science and Technology (KAUST). His current research interest includes signal processing-based features generation for biomedical signal classification and prediction.

SOURAV BHADURI received the M.Sc. degree in information technology with specialization in communication engineering and media technology from the University of Stuttgart, Germany, in 2013. He is currently pursuing the Ph.D. degree in health sciences with Ghent University, Belgium. From 2014 to 2015, he was a Senior R&D Engineer with the National Brain Research Centre, India. He is involved in development and validation of high-speed pulse sequence and post processing methods for magnetic resonance spectroscopic imaging. His research interests include biomedical signal processing, medical physics, applied math, and machine learning.

MOHAMED MAOUI received the B.Eng. degree in electrical and electronics engineering from the Ecole Nationale Polytechnique, Algiers, Algeria, in 2018. He is currently pursuing the M.Eng. degree in biomedical engineering with the Micro and Nanobioengineering Laboratory, Faculty of Medicine and Engineering, McGill University, Montreal, Canada. His current research consists of applying different biostatistical and artificial intelligence approaches in order to develop new computational and image analysis techniques to investigate and characterize single exosomes, all to improve the robust detection of rare species, such as exosomal RNA and cancer-derived proteins, which eventually leads to achieving a better understanding of tumors growth and invasion. In 2018, he received the Abdullah AlGhurair Foundation for Education AGFE Fellowship to pursue the graduate studies at McGill University. In 2019, he was selected as an AGFE Ambassador for the AGFE Scholars in Canada and USA, the Leader to promote research in the Arab World, an Advocate for mental health, and other values.

ERIC ACHTEN received the Medical degree from the Free University of Brussels, in 1982, and the Ph.D. degree, in 1998. His Ph.D. topic was on MR imaging and spectroscopy in the diagnosis of epilepsy. He has been specialized in nuclear medicine and radiology from the Free University of Brussels. He has been a certified Radiologist with a specialization in neuroradiology. Since 1990, he has been a Neuroradiologist with the Ghent University Hospital. Since 2000, he has also been a Professor in neuroradiology with Ghent University, Belgium. Since 2011, he has been the Head of medical imaging. Many research projects and collaborations resulted in over 200 publications (http://scholar.google.com/citations?user=R8EiuQkAAAAJ&hl=en).

HACENE SERRAI received the master's degree in biomedical signal and image processing from the University of Tours, France, and the Ph.D. degree in biomedical signal and image processing from the University of Rennes, France. After completing the Postdoctoral Fellowship at the University of Pennsylvania, Philadelphia, he joined as a Research Officer with IBD–NRC, Winnipeg, Canada, in 2002. In 2014, he moved to Ghent University, Belgium, for three years, as a Medical Physicist. He joined CFMM as a Research Scientist, in 2017. His current researches focus on the development, implementation, and validation of arterial spin labeling and high-speed MRSI sequences at high field.

TAOUS-MERIEM LALEG-KIRATI received the Ph.D. degree in applied mathematics from INRIA, Paris, in 2008, and the master's degree in control systems and signal processing from the University of Paris XI, France. From 2009 to 2010, she was a permanent Research Scientist with the French Institute for Research in Computer Sciences and Control Systems, INRIA, Bordeaux. In 2010, she joined as an Associate Professor with the Division of Computer, Electrical and Mathematical Sciences and Engineering, King Abdullah University of Science and Technology. Her research interests include modeling, estimation, and control of complex systems and signal/image analysis. She considers applications in engineering and biomedical fields.